4252–4265 *Nucleic Acids Research, 2016, Vol. 44, No. 9* *Published online 11 April 2016*
doi: 10.1093/nar/gkw240

DHX29 reduces leaky scanning through an upstream AUG codon regardless of its nucleotide context

Vera P. Pisareva* **and Andrey V. Pisarev***

Department of Cell Biology, SUNY Downstate Medical Center, 450 Clarkson Ave, Brooklyn, NY 11203, USA

Received November 24, 2015; Revised March 25, 2016; Accepted March 29, 2016

ABSTRACT

During eukaryotic translation initiation, the 43S preinitiation complex (43S PIC), consisting of the 40S ribosomal subunit, eukaryotic initiation factors (eIFs) and initiator tRNA scans mRNA to find an appropriate start codon. Key roles in the accuracy of initiation codon selection belong to eIF1 and eIF1A, whereas the mammalian-specific DHX29 helicase substantially contributes to ribosomal scanning of structured mRNAs. Here, we show that DHX29 stimulates the recognition of the AUG codon but not the near-cognate CUG codon regardless of its nucleotide context during ribosomal scanning. The stimulatory effect depends on the contact between DHX29 and eIF1A. The unique DHX29 N-terminal domain binds to the ribosomal site near the mRNA entrance, where it contacts the eIF1A OB domain. UV crosslinking assays revealed that DHX29 may rearrange eIF1A and eIF2α in key nucleotide context positions of ribosomal complexes. Interestingly, DHX29 impedes the 48S initiation complex formation in the absence of eIF1A perhaps due to forming a physical barrier that prevents the 43S PIC from loading onto mRNA. Mutational analysis allowed us to split the mRNA unwinding and codon selection activities of DHX29. Thus, DHX29 is another example of an initiation factor contributing to start codon selection.

INTRODUCTION

Eukaryotic translation consists of four stages: initiation, elongation, termination and ribosomal recycling. The first stage, initiation, is the most complex and the most regulated (1,2). It starts with the assembly of the ternary complex (TC), consisting of eIF2, GTP and aminoacylated initiator Met-tRNA$_i^{Met}$. TC, in cooperation with eIF3, eIF1 and eIF1A, binds to the 40S ribosomal subunit, forming the 43S preinitiation complex (43S PIC). eIF1 and eIF1A synergistically associate with the 40S subunit (3). eIF1 binds adjacent to the P site, whereas eIF1A primarily binds to the A site (4,5). Upon binding, eIF1 and eIF1A cooperatively induce the rearrangement of the 40S subunit from a closed scanning-arrested state to an open scanning-competent state (6). Such a conformational change underlies the mechanism by which these factors secure the fidelity of initiation codon selection. The position of eIF1 close to the P site, along with its conserved basic β hairpin loop 1 protruding toward the mRNA cleft at the P site, physically prevent imperfect mRNA codon and initiator tRNA anticodon base pairing (4,5,7). eIF1A consists of a central oligonucleotide/oligosaccharide-binding (OB) domain, which is responsible for binding to the 40S subunit (4,5), and long, unstructured terminal tails. The C-terminal tail (CTT) of eIF1A, which is thought to sterically occlude initiator tRNA access to the P site, plays an important role in the stabilization of the open scanning-competent conformation of the 43S PIC (8). In turn, the N-terminal tail (NTT) of eIF1A, through direct interactions with anticodons, mRNA and rRNA, stimulates the transition from a scanning-competent to a scanning-arrested conformation of the 43S PIC, favoring initiation codon recognition (9).

After assembly, the 43S PIC is loaded onto the 5′ end of mRNA preliminarily unwound by eIFs 4A, 4B and 4F. After mRNA attachment, the open-state 43S PIC scans the 5′-untranslated region (5′-UTR) of the mRNA downstream to the appropriate start codon, where it stops and forms the 48S initiation complex (48S IC). In addition to its activity in 43S PIC loading onto the mRNA, eIF4A is thought to be responsible for mRNA secondary structure unwinding during ribosomal scanning. According to the statistical analysis, the majority of mammalian mRNAs contain moderately to extensively structured 5′-UTRs (10). The mammalian-specific DExH-box helicase DHX29 substantially contributes to 48S IC formation on structured mRNAs in vitro and *in vivo* (10,11). DHX29 contains a unique N-terminal region, a centrally located helicase domain, and a C-terminal region containing helicase-associated 2 (HA2) and OB domains. Recent CryoEM data revealed the position of DHX29 in the 43S PIC (12). The central and C-terminal regions of DHX29 are located around the tip of helix H16 of the 40S subunit. The distal part extends along

*To whom correspondence should be addressed. Tel: +1 718 270 1143; Fax: +1 718 270 2656; Email: andrey.pisarev@downstate.edu
Correspondence may also be addressed to Vera P. Pisareva. Email: vera.pisarev@downstate.edu

the mRNA entry channel and enters the intersubunit interface up to the eIF1A-binding site, where it bridges the body and the beak of the 40S subunit near the mRNA entry channel latch (12). Despite these novel structural data, the mechanism of the RNA unwinding activity of DHX29 remains obscure.

Start codon recognition is accompanied by the establishment of mRNA codon and Met-tRNA$_i^{Met}$ anticodon base pairing. Importantly, the efficiency of 48S IC formation during ribosomal scanning depends on the nucleotide context of the AUG codon. The strongest context is (A/G)CCAUGG, where purines at the '−3' and '+4' positions relative to the A in AUG are the most critical (13). Studies with yeast factors have revealed that the formation of codon-anticodon interaction causes the dissociation of eIF1 and the rearrangement of the 40S subunit into the closed scanning-arrested state (6,14–17).

A large-scale analysis of human mRNAs indicates that only 38% of mRNAs contain an annotated start codon in the optimal Kozak context. Of the remaining mRNAs, 52% and 10% are in suboptimal and non-optimal Kozak contexts, respectively, suggesting lower translation efficiencies of these mRNAs (18,19). However, high-throughput sequencing experiments have indicated that the majority of mRNAs in suboptimal nucleotide contexts are translated as efficiently as mRNAs in the optimal context (18). Mutations in the Kozak context have the potential to change the efficiency of AUG recognition, thereby disrupting protein translation levels and impacting human health (20,21). Indeed, several nucleotide context mutations are associated with tumorigenesis (22). Therefore, this topic relates to public health. Efficient translation initiation at annotated AUG codons in the suboptimal context suggests that the Kozak context rule is not universal, and additional factors can affect translation initiation efficiency. Accordingly, it was recently shown that eIF3j, eIF5 and eIF5B modulate the efficiency of start codon selection (23–26).

Notably, many mRNAs (37-49%) in mammals contain at least one uAUG codon (27). Scanning ribosomal complexes reach the annotated AUG codon via either a leaky scanning mechanism bypassing uAUGs or a reinitiation mechanism after the translation of upstream ORFs (uORFs) (28–30). At the same time, initiation on uAUGs results in the formation of alternative proteins, in-frame or out-of-frame with the annotated protein, which play important roles in cell viability (27). As a result, the discovery of protein factors influencing AUG selection and understanding the mechanism of their activity become critically important in light of the established connection between the efficiency of initiation codon selection and human health.

Although both yeasts and mammals are eukaryotes, yeasts are unicellular, whereas mammals are multicellular organisms with more complex translation regulation mechanisms. To mediate this regulation, mammalian cells employ mammalian-specific protein factors, such as DHX29. Moreover, the optimal AUG context differs between yeast and mammals, and the 5′-UTRs of mRNAs are less structured in yeast than in mammals. Therefore, although yeast genetics is a powerful approach, it cannot describe the entire picture of translation regulation in mammals. Hence the work with mammalian factors is very much needed and in this respect the well established mammalian in vitro reconstituted system has provided invaluable help in solving this problem in the past on many occasions (11,31).

eIF3j and part of DHX29 occupy the same position on the 40S subunit in close proximity to eIF1A (32). There is evidence of a functional interaction between eIF3j and eIF1A in stringent AUG selection in yeast (23), suggesting the potential involvement of DHX29 in initiation codon selection. Here, we tested this suggestion employing the aforementioned mammalian reconstituted in vitro system and found that DHX29 decreases leaky scanning through an upstream AUG codon (uAUG) but not a near-cognate CUG codon regardless of the Kozak context. We also detected direct contact between the N-terminal part of DHX29 and the OB domain of eIF1A. This contact is essential for the reduced leaky scanning through AUG in the presence of DHX29 but has no influence on the RNA unwinding activity of protein during ribosomal scanning. Therefore, we discovered and characterized the novel activity of DHX29 in translation initiation. Our findings help to explain the recently described discrepancies with the classical Kozak context rule. The mechanism underlying the observed effect is discussed.

MATERIALS AND METHODS

Plasmids

Expression vectors for His$_6$-tagged eIFs 1, 1A, 4A, 4B and *Escherichia coli* methionyl-tRNA synthetase and transcription vectors for TC, AC and AG mRNAs, (AUG at -6)-Stem mRNA and tRNA$_i^{Met}$ have been described (11,24,33–35). Vectors for the expression of all DHX29 deletion mutants and eIF1A substitution mutants were constructed by site-directed mutagenesis of DHX29 and eIF1A expression vectors, respectively. Expression vectors for GST-tagged DHX29(FL) and eIF1A(FL) were prepared by cloning the corresponding protein coding region following a GST-tag into the *BamHI*/*XhoI* sites of pGEX-6P-1. Vectors for the expression of GST-tagged DHX29 and eIF1A deletion mutants were constructed by site-directed mutagenesis of GST-DHX29(FL) and GST-eIF1A(FL) expression vectors, respectively. Transcription vectors for '-3U' and '+4U' mRNAs were made by inserting the corresponding DNA following a T7 promoter into the *PstI*/*SmaI* sites of pUC19. The transcription vector CUG-AUG was constructed via the site-directed mutagenesis of the AG mRNA plasmid. mRNAs and tRNA$_i^{Met}$ were transcribed using T7 RNA polymerase. All mRNA transcripts were capped with Vaccinia virus capping enzyme (NEB) according to the manufacturer's protocol. Radiolabeled '-3U' and '+4U' mRNAs containing 4-thioU were obtained by transcription in the presence of [α-32P]CTP and 4-thioU (TriLink Biotech).

Antibodies

We used DHX29 antibodies (Bethyl Laboratories and Cell Signaling Technology) and eIF1A antibodies (GeneTex).

Purification of translation components and aminoacylation of tRNA

Native 40S subunits, eIFs 2/3/4F, recombinant eIFs 1/1A/4A/4B and *E. coli* methionyl-tRNA synthetase were purified as described (11,33,34). Native β-globin mRNA was purified from 10 ml rabbit reticulocyte lysate (Green Hectares) on poly(dT)-agarose (NEB) according to the manufacturer's protocol. *In vitro* transcribed $tRNA_i^{Met}$ and rabbit native total tRNAs (Promega) were aminoacylated with methionine in the presence of recombinant *E.coli* methionyl-tRNA synthetase as described (11).

Purification of DHX29 WT form and mutants

Recombinant DHX29(WT), DHX29(Δ1-24), DHX29(Δ1-53), DHX29(Δ1-90), DHX29(Δ1-124), DHX29(Δ61-90), DHX29(Δ121-150) and DHX29(Δ181-210) were expressed in 4 l of *E. coli* BL21(DE3) each after induction by 0.1 mM IPTG for 16 h at 16°C. Soluble proteins were isolated by affinity chromatography on Ni-NTA agarose followed by fast protein liquid chromatography (FPLC) on a MonoS column. Fractions were collected across a 100–500 mM KCl gradient. DHX29(WT) was eluted at 310 mM, DHX29(Δ1–24) and DHX29(Δ1–53) at 140 mM, DHX29(Δ181–210) at 280 mM KCl. DHX29(Δ1–90), DHX29(Δ1–124), DHX29(Δ61–90) and DHX29(Δ121–150) were found insoluble after expression, so we did not proceed with purification.

eIF1A mutants purification

Recombinant eIF1A(7–11→5A), eIF1A(12–16→5A), and eIF1A(17–21→5A) were expressed in 1 l of *E. coli* BL21(DE3) after induction by 1 mM IPTG for 5 h at 37°C and isolated by affinity chromatography on Ni-NTA agarose followed by FPLC on a MonoQ column. Fractions were collected across a 100–500 mM KCl gradient. All mutants were eluted at 320 mM KCl.

GST-tagged protein lysate preparation for GST pull-down assay

Recombinant GST-DHX29(FL), GST-DHX29(1–247), GST-DHX29(248–594), and GST-DHX29(595–1369) as well as GST-eIF1A(FL), GST-eIF1A(NTT), GST-eIF1A(OB) and GST-eIF1A(CTT) proteins for GST pull-down assay were prepared in the form of *E. coli* lysates by the same protocol. Each protein was expressed in 1 l of *E. coli* BL21(DE3) after induction by 0.1 mM IPTG for 16 h at 16°C. Cells were collected, lysed in 20 ml buffer B (20 mM Tris–HCl, pH 7.5, 100 mM KCl, 0.1 mM EDTA, 10% glycerol) by sonication, clarified from cell debris by 10′ 15k rpm centrifugation, and frozen at −80°C for the downstream assay.

Assembly of initiation complexes

To reconstitute 48S IC, we incubated different combinations of 0.2–2 pmol DHX29 (WT or mutants), 5 pmol eIFs 2/3/4F, 7 pmol eIFs 1/1A(WT or mutants)/4A/4B, 5 pmol Met-$tRNA_i^{Met}$ (native or transcript), and 1.75 pmol 40S ribosomal subunit in a 20 μl reaction mixture containing buffer A (20 mM Tris–HCl, pH 7.5, 100 mM KCl, 2.5 mM $MgCl_2$, 0.1 mM EDTA, 1 mM DTT) with 0.2 mM ATP and 0.2 mM GTP for 10 min at 37°C in the presence of 0.3 pmol corresponding mRNA.

Toeprint assay

We estimated the yields of 48S ICs assembled on different mRNAs by employing the toeprint assay as described (11). This assay involves the extension of a radiolabeled primer annealed to the mRNA by reverse transcriptase. Generally, ribosomal complexes yield toeprint signals at the leading edge of the 40S subunits at the position +16 to +18 nt downstream of the mRNA triplet in the P site. Signals are visualized after the electrophoresis of cDNA in denatured polyacrylamide gels and autoradiography.

UV crosslinking assay

To examine the effect of DHX29 on the rearrangement of initiation complexes, we performed UV crosslinking experiments. The 48S ICs were reconstituted with/without DHX29 and eIF1A on co-transcriptionally 32P-labeled '−3U' and '+4U' mRNAs containing 4-thioU at the −3 and +4 key context positions, respectively. To maintain the integrity of ribosomal complexes, we omitted the purification step by SDG centrifugation. After assembly, the 48S ICs were irradiated at 360 nm for 30 min on ice using a UV Crosslinker (Spectroline) and were then digested with 5 units RNase A for 10 min at 37°C. To identify crosslinked proteins, ribosomal complexes were assayed by SDS-PAGE and autoradiography.

GST pull-down assay

To study the interaction between DHX29 and eIF1A, we employed GST pull-down assays. GST-tagged protein was preliminary bound to Glutathione Sepharose 4B (GE Healthcare) and incubated with the purified recombinant partner. The complex was eluted with 1× loading buffer (Life Sciences), resolved via denatured SDS-PAGE, and analyzed by immunoblotting.

RESULTS

DHX29 reduces leaky scanning through an upstream AUG codon but not a near-cognate CUG codon regardless of Kozak context on model mRNAs in the mammalian reconstituted system

To evaluate the influence of DHX29 on the efficiency of AUG codon selection in the reconstituted system, we assembled 48S ICs from 40S ribosomal subunits, eIFs 1, 1A, 2, 3, 4A, 4B, 4F and aminoacylated initiator Met-$tRNA_i^{Met}$ on model mRNA in the presence of the protein in question. The model mRNA (TC mRNA) was previously described (24) and consists of a single-stranded 5′-UTR followed by two initiation codons separated by a 12 nt single-stranded region (Figure 1A). The first AUG codon is in a poor nucleotide context (with T and C pyrimidines in the '−3' and '+4' key positions, respectively), whereas the second AUG

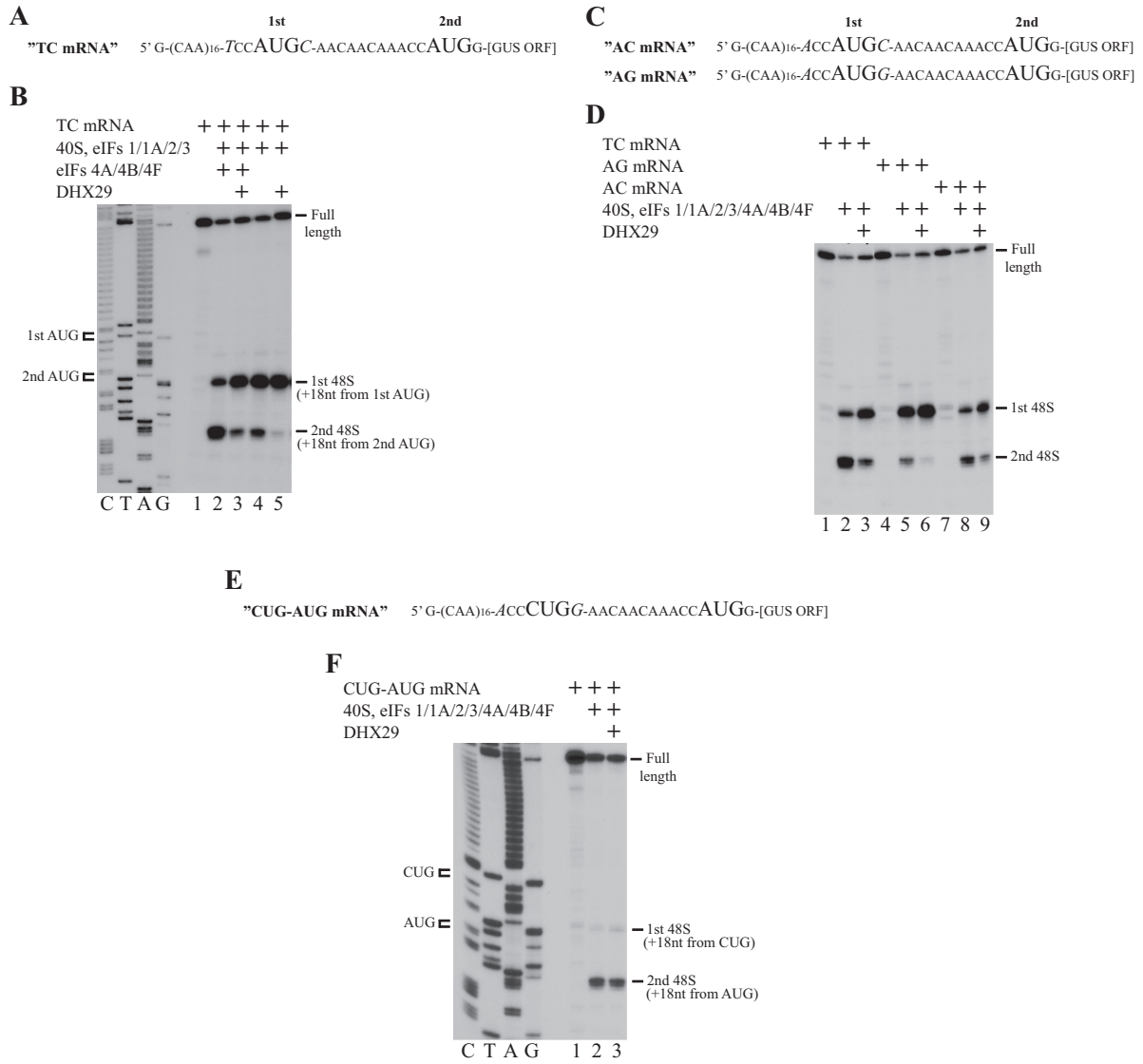

Figure 1. DHX29 affects AUG recognition regardless of nucleotide context. (**A**) Structure of TC mRNA. (**B**) Toeprint analysis of 48S IC assembly on TC mRNA in the presence of DHX29. Initiation codons and positions of the assembled 48S IC are indicated. Lanes C/T/A/G depict corresponding DNA sequences. (**C**) Structures of AC and AG mRNAs. (**D**) Toeprint analysis of 48S IC assembly on TC, AC and AG mRNAs in the presence of DHX29. Positions of full-length signal and assembled ribosomal complexes are indicated. (**E**) Structure of CUG-AUG mRNA. (**F**) Toeprint analysis of 48S IC formation on CUG-AUG mRNA in the presence of DHX29. Initiation codons and positions of the reconstituted 48S IC are shown. Lanes C/T/A/G depict corresponding DNA sequences.

codon is in the optimal context. The second start codon is linked with the β-glucuronidase open reading frame (ORF). The position and assembly efficiency of 48S IC were analyzed by toeprint assay. Generally, ribosomal complexes yield toeprint signals at the position +16 to +18 nt downstream of the mRNA triplet in the P site of the 40S subunit. As expected, in the presence of a canonical set of factors, scanning ribosomal complexes predominantly passed the first AUG codon and formed the 48S IC on the second (Figure 1B, lanes 1 and 2). DHX29 supplementation resulted in the formation of the 48S IC mainly on the first AUG codon (Figure 1B, lane 3). Therefore, DHX29 in our system reduces the capacity of the 43S PIC to discriminate against poor Kozak context for AUG codons during ribosomal scanning.

To exclude the role of eIFs 4A, 4B and 4F in the DHX29-mediated effect, we removed these factors from the system. The omission of proteins decreased the processivity of scanning ribosomal complexes, resulting in the formation of the 48S IC predominantly on the first AUG codon (Figure 1B, lane 4). Since, the addition of DHX29 further reduced leaky scanning through the first AUG codon (Figure 1B, lane 5), we conclude that eIFs 4A, 4B and 4F are dispensable for the effect.

To evaluate the dependence of DHX29 activity on the AUG nucleotide context of mRNA, we compared 48S IC assembly on AC, AG and TC mRNAs. The two former mRNAs were similar to TC mRNA, but the first AUG codon was in a sub-optimal context in AC mRNA (with A purine and C pyrimidine in the '−3' and '+4' key positions, respec-

tively) and in an optimal context in AG mRNA (A and G purines in the key positions) (Figure 1C). Despite the different distributions of the 48S ICs between start codons in the presence of canonical factors, DHX29 stimulated 48S IC formation on the first AUG codon for all mRNAs (Figure 1D). Therefore, DHX29 activity does not depend on the AUG nucleotide context.

We next assayed the role of DHX29 in near-cognate CUG codon recognition during ribosomal scanning. To obtain CUG-AUG mRNA, we replaced the first AUG codon in TC mRNA with the near-cognate CUG codon in the optimal nucleotide context (Figure 1E). DHX29 did not affect 48S IC formation on the upstream CUG codon of CUG-AUG mRNA (Figure 1F). Therefore, DHX29 reduces leaky scanning through an upstream AUG codon but not through a near-cognate CUG codon regardless of nucleotide context.

N-terminal DHX29 makes direct contact with the OB domain of eIF1A

Recently published CryoEM data on the ribosomal position of DHX29 in the mammalian 43S PIC revealed that DHX29 binds around the tip of helix H16 of the 40S subunit and contacts eIF3 (12). Modeling of eIF1A on the 40S subunit placed its OB domain in close proximity to the distal part of DHX29 (12). We employed GST pull-down assays to test whether DHX29 and eIF1A establish direct contact. We hypothesized that the distal density of DHX29 by size could correspond to the N-terminal part of the protein and constructed three GST-tagged DHX29 deletion mutants consisting of aa 1–247, 248–594 and 595–1369, along with the full-length (FL) form (Figure 2A). eIF1A interacted strongly with GST-DHX29(FL) and GST-DHX29(1–247) and weakly also with the other two DHX29 variants (Figure 2B).

To localize the contact site on eIF1A, we divided the protein according to its domain organization. We prepared three GST-tagged mutants, consisting of aa 1–31 (NTT), 32–95 (OB) and 96–144 (CTT), along with the 1–144 (FL) form (Figure 2C). In GST pull-down assays, DHX29 interacted with GST-eIF1A(FL) and GST-eIF1A(OB) (Figure 2D). These results are in good agreement with the modeled positions of the proteins in the 43S PIC (12). Therefore, the distal density of DHX29 on the 40S subunit, which has not been assigned to any particular part of DHX29 to date, is attributed to the N-terminal region of the protein.

DHX29 does not cause the dissociation of eIF1 or eIF1A from 43S PIC during ribosomal scanning

eIF1 and eIF1A are key players in the fidelity of start codon selection during ribosomal scanning. Despite the existence of direct contact between DHX29 and eIF1A, the discovered activity of DHX29 may be explained by the dissociation of eIF1 or eIF1A upon DHX29 binding to the 43S PIC. eIF1 serves as the major Kozak context discriminator (36), and its absence could explain the failure of the DHX29-containing 43S PIC to discriminate against poor AUG context. The reduced capacity of the scanning 43S PIC to discriminate against non-optimal AUG context in the reconstituted system was also shown upon omission of eIF1A (37). To date, the canonical set of initiation factors permits efficient 48S IC formation in the mammalian reconstituted system only on either β-globin mRNA or model mRNA with single-stranded 5′-UTRs. Therefore, we assayed the role of eIF1 and eIF1A in the DHX29-mediated effects on these mRNAs by the omission of either factor from the reconstituted system. The 43S PIC is arrested at different characteristic positions along the β-globin mRNA during ribosomal scanning in the absence of either eIF1 or eIF1A (36,37). Consistently, without eIF1A in the system, the 48S IC assembled on the AUG start codon and the preceding near-cognate CUG codon (Figure 3A, lane 1). Note the background signals that are present in the control obtained in the absence of factors (Figure 3A, lane 5). The 40S ribosomal subunits in our reconstituted system were purified from RRL containing large amounts of β-globin mRNA. Despite the rigorous purification protocol, 40S subunits cannot be purified absolutely free of mRNA and are always somewhat contaminated with β-globin mRNA and initiator tRNA, which are presumably stabilized by codon-anticodon interactions in the P site resulting in the background toeprint signal. To estimate the contribution of this signal in 48S IC formation efficiency on β-globin mRNA, we show the control lane 5 containing purified 40S subunits only (Figure 3A, lane 5). The omission of eIF1 caused even more dramatic effects. The 43S PIC loaded onto mRNA but could not scan downstream, yielding the toeprint at the position +21 to +24 nt from the 5′ end of the mRNA (Figure 3A, lane 2). The simultaneous removal of both factors resulted in the absence of specific toeprint signals (Figure 3A, lane 3). The addition of DHX29 to the system with the full set of factors led to the only strong toeprint signal, which corresponded to the 48S IC assembled on the AUG start codon (Figure 3A, lane 4). Importantly, 48S IC formation on the annotated AUG of native β-globin mRNA in the reconstituted system strictly requires the presence of both eIFs 1 and 1A (36). In the absence of either factor in our experiment, the scanning 43S PIC did not reach the AUG codon, forming characteristic aberrant toeprint signals (Figure 3A, lanes 1 and 2) that were consistent with published data (36), suggesting that the open scanning-competent conformation of the ribosomal complex is critical for efficient 48S IC formation. If DHX29 caused the dissociation of either or both factors, we would obtain the corresponding toeprint profile. However, DHX29 in the presence of the full set of factors resulted in 48S IC formation on the annotated AUG codon and did not produce characteristic aberrant toeprint signals. This observation allowed us to conclude that the DHX29 stimulatory effect is not linked to the dissociation of either or both of these factors from the 43S PIC during ribosomal scanning.

In the toeprint experiment on TC mRNA, the removal of eIF1A generally led to 48S IC formation on the first AUG codon (Figure 3B, lanes 1–3, and 6). Surprisingly, the presence of DHX29 did not permit 48S IC assembly at any codon (Figure 3B, lane 7). Importantly, our finding is not a result of DHX29-induced eIF1 dissociation, as the 48S IC can be assembled on single-stranded mRNA even in the absence of both eIF1 and eIF1A (37). This observation could be explained by findings from CryoEM data on DHX29 in the 43S PIC. The distal part of DHX29 bridges the body

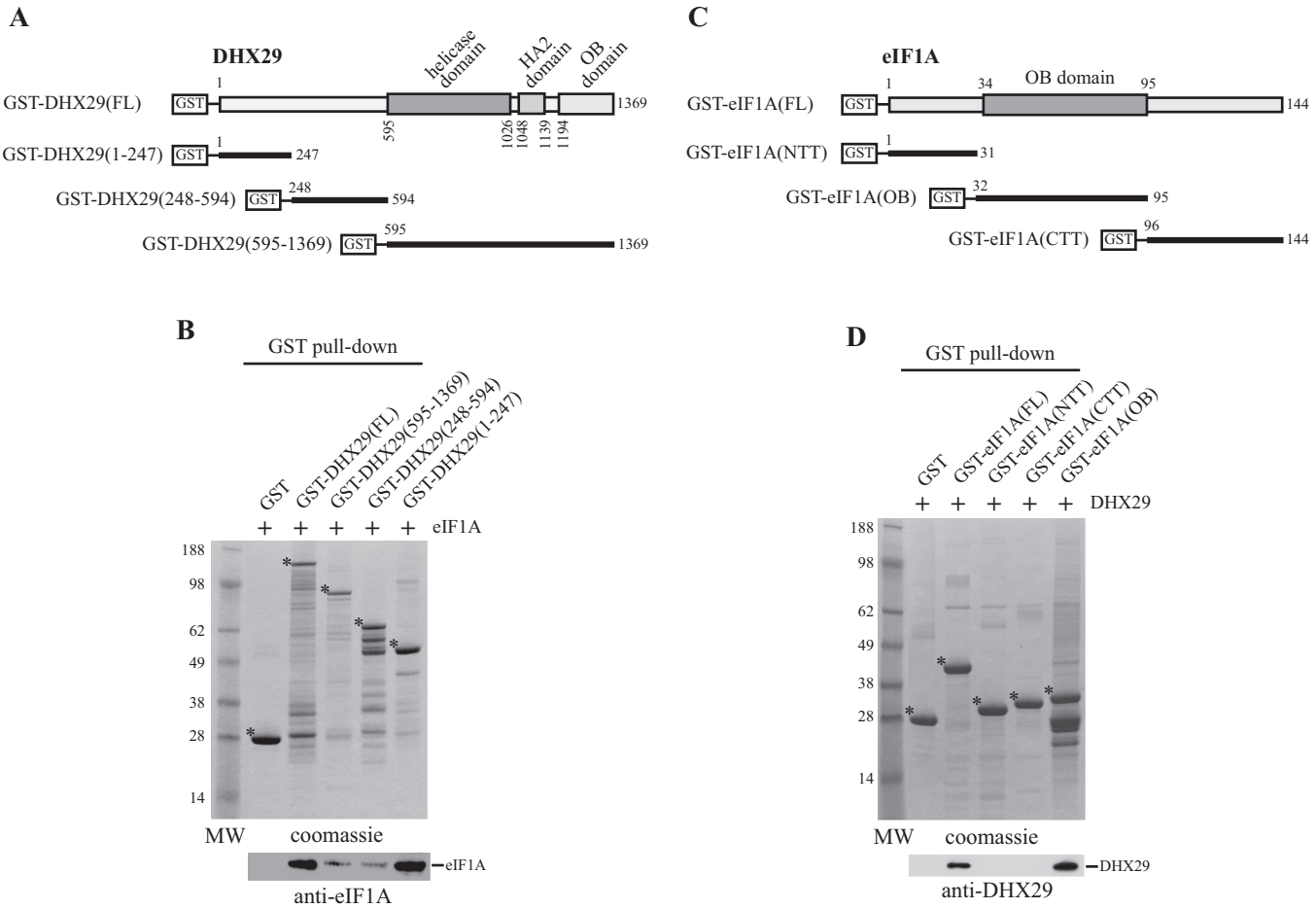

Figure 2. Interaction between DHX29 and eIF1A. (**A** and **C**) GST-tagged (A) DHX29 and (C) eIF1A and their fragments used in the GST pull-down assay. (**B** and **D**) Binding of (B) different fragments of DHX29 to eIF1A and (D) different fragments of eIF1A to DHX29, as analyzed by GST pull-down assay. An aliquot of each binding reaction after elution from glutathione resin was assayed by SDS-PAGE and either Coomassie blue staining or immunoblotting. The asterisks indicate the main bands of GST-tagged fragments. Positions of molecular weight markers are shown.

and the beak of the 40S subunit near the mRNA entry channel latch (12). The obtained CryoEM image does not contain eIF1 and eIF1A. Therefore, this arrangement could be the scenario in our reconstituted system. In the absence of eIF1A, DHX29 establishes the described bridge, creating the physical barrier and preventing the 43S PIC from loading onto mRNA. Because DHX29 in the absence of eIF1A impairs 48S IC formation, it cannot affect start codon selection through eIF1A dissociation. In turn, the removal of eIF1 resulted in 48S IC assembly only on the first AUG codon (Figure 3B, lane 4). The addition of DHX29 caused slight leaky scanning, with minor 48S IC formation on the second AUG codon (Figure 3B, lane 5). This effect may be explained by the helicase activity of DHX29. Indeed, in the absence of eIFs 4A/4B/4F, the 43S PIC cannot efficiently scan downstream of the first AUG codon of TC mRNA due to impaired unwinding activity (Figure 1B, lane 4). Notably, the formation of the 48S IC exclusively on the first AUG codon in the absence of eIF1 and mostly on the first AUG codon in the absence of eIF1A are consistent with the reported strict and more modest discrimination roles of eIF1 and eIF1A, respectively, in the fidelity of initiation codon selection (1).

Because DHX29 prevents 48S IC formation on TC mRNA in the absence of eIF1A, in the next experiment we assayed whether DHX29 exhibited the same activity on β-globin mRNA. Consistent with the result obtained for TC mRNA, in the absence of eIF1A, DHX29 prevented 48S IC formation at any codon of β-globin mRNA (Figure 3C, lanes 1–4), confirming the uniformity of the effect on different mRNAs. The addition of DHX29 in the absence of eIFs 1 and 1A did not affect the toeprint pattern on the native β-globin mRNA (Figure 3C, lanes 5 and 6). Interestingly, the described above background signal (Figure 3A, lane 5) is eliminated by DHX29 in the absence of eIF1A (Figure 3C, lane 4). It was previously reported that eIF1 ejects the P-site deacylated tRNA from 40S/mRNA/tRNA complexes during ribosomal recycling in the mammalian reconstituted system. This weakens the 40S/mRNA stability resulting in final dissociation of components (33). We suggest that this activity of eIF1 could be responsible for the dissociation of 40S/β-globin mRNA/initiator tRNA complex in our experiment, whereas DHX29 in the absence of eIF1A could prevent 43S PIC loading onto mRNA resulting in the reduction of the background signal in the lane (Figure 3C, lane 4). Consistently, upon the removal of eIF1 from this

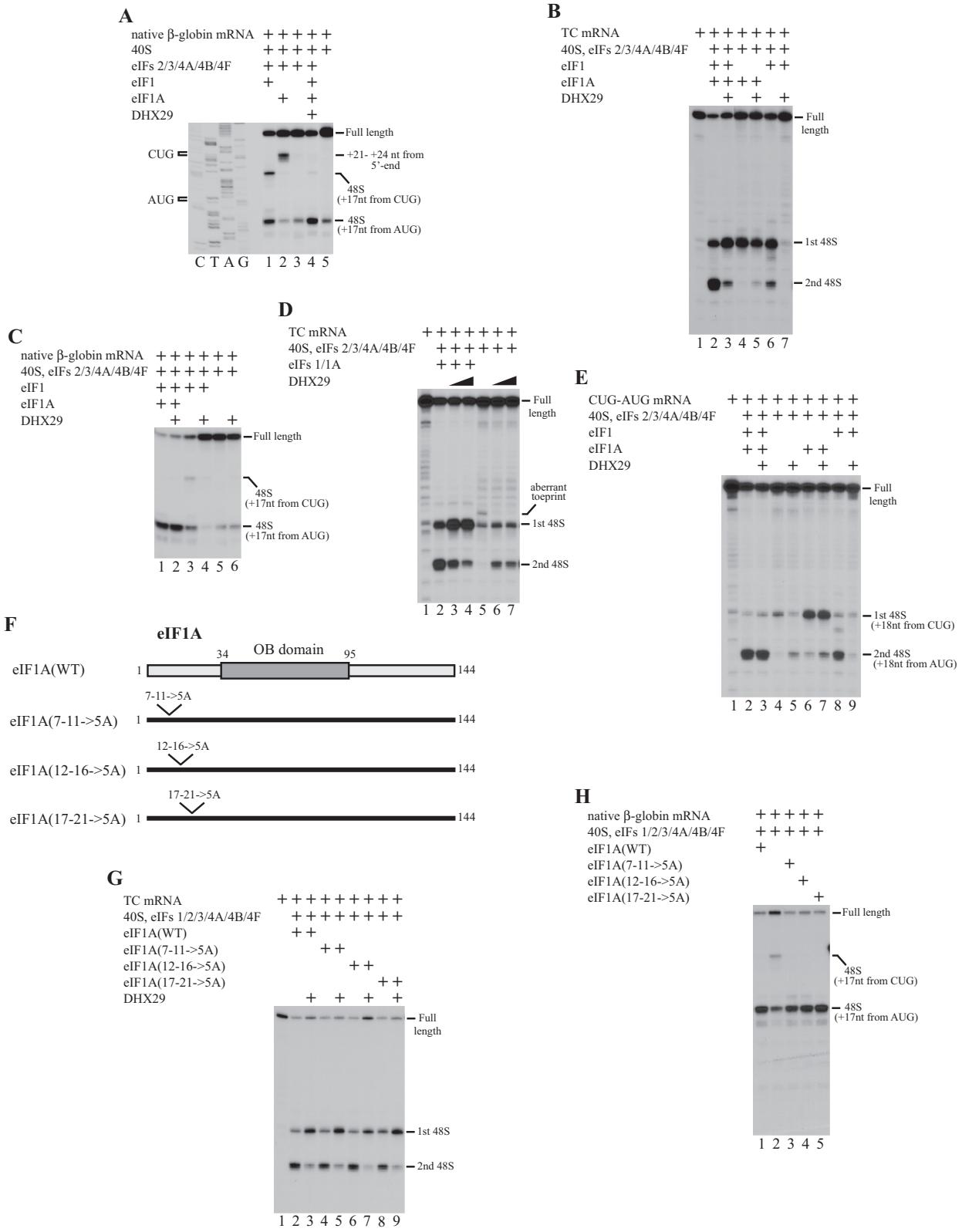

Figure 3. Interplay between DHX29 and eIFs 1 and 1A in 48S IC formation on different mRNAs. Role of the eIF1A NTT in DHX29-mediated AUG selection. (**A–E**) Toeprint analysis of 48S IC assembly on (A, C) native β-globin, (B, D) TC and (E) CUG-AUG mRNAs in the presence of different combinations of DHX29, eIF1, and eIF1A. Initiation codons and positions of the assembled 48S ICs are indicated. Lanes C/T/A/G depict corresponding DNA sequences. (**F**) Location of substitution mutations in the eIF1A NTT. (**G–H**) Toeprint analysis of 48S IC formation on (G) TC and (H) native β-globin mRNAs in the presence of different combinations of eIF1A mutants and DHX29. Positions of full-length signal and the assembled 48S ICs are indicated.

reaction, the background signal is not decreased regardless the presence of DHX29 (Figure 3C, lanes 5 and 6). On the other hand, in contrast to the reconstitution in the system with the full set of factors, in the absence of eIFs 1 and 1A, the 48S IC was assembled inefficiently and exclusively on the first AUG codon of TC mRNA (Figure 3D, lanes 1, 2 and 5). Although DHX29 in the full system stimulated AUG recognition in a concentration-dependent manner, in the absence of eIFs 1 and 1A, it increased leaky scanning through the first AUG codon with the same efficiency at different concentrations (Figure 3D). Notice the aberrant toeprint signal, presumably representing the 48S IC assembled on the first AUG with improperly positioned mRNA in the mRNA entry channel, which disappeared in the presence of DHX29, as previously described (Figure 3D, lanes 5–7) (11). Taking into account these data, we conclude that DHX29 does not stimulate AUG recognition in the absence of eIFs 1 and 1A.

For more insight into the mechanism of DHX29 activity, we assayed the interplay between DHX29 and eIFs 1 and 1A in 48S IC formation on CUG-AUG mRNA. Compared to the full set of canonical factors, the 48S IC in the absence of eIF1 was mostly assembled on the first near-cognate CUG codon of CUG-AUG mRNA, which was consistent with the strict codon-discrimination role of the protein (Figure 3E, lanes 1, 2 and 6). Importantly, the addition of DHX29 to the system with the full set of factors did not reduce leaky scanning through the near-cognate CUG codon, indicating that the codon-discrimination activity of ribosomal complexes in the presence of DHX29 is not decreased (Figure 3E, lanes 1–3 and 6). This result suggests that the key codon-discriminating protein eIF1 is not dissociated. As with the absence of eIF1, the removal of both eIFs 1 and 1A resulted in inefficient 48S IC assembly on the first near-cognate CUG codon (Figure 3E, lane 4). The addition of DHX29 to the system without either eIF1 alone or eIFs 1 and 1A together increased leaky scanning through the CUG codon, as we observed on TC mRNA (Figure 3E, lanes 5 and 7). Finally, in the absence of eIF1A, DHX29 did not permit 48S IC assembly at any CUG-AUG mRNA codon, confirming the universality of the inhibitory effect (Figure 3E, lanes 8 and 9).

Mammalian eIF1A NTT does not contribute to codon recognition in the reconstituted system

Based on our findings, we hypothesized that DHX29 influences start codon selection through contact with eIF1A. Highly homologous between mammals and yeast, eIF1A directly affects AUG selection through its terminal tails in opposite manners. The eIF1A CTT stabilizes an open scanning-competent conformation of the 43S PIC, whereas the eIF1A NTT stimulates the transition from an open conformation to a closed scanning-arrested conformation of the ribosomal complex, enhancing AUG recognition. Recent CryoEM data revealed that the eIF1A NTT makes contacts with the AUG codon, the anticodon, the '+4' key context nucleotide in mRNA, and rRNA in the partial yeast 48S IC (9). These data confirmed previous biochemical and genetic findings implicating eIF1A NTT residues between positions 7 and 21 in stimulating the isomerization from an open to a closed conformation of the 43S PIC for AUG recognition (8,38,39). Therefore, we evaluated the role of the eIF1A NTT in AUG recognition in our system and tested whether DHX29 acts through the eIF1A NTT. We constructed three substitution mutants of mammalian eIF1A, replacing residues in the NTT between positions 7 and 11, 12 and 16, or 17 and 21 with five alanines (Figure 3F), similar to the yeast eIF1A mutants that impair AUG recognition in vivo (38). eIF1A mutations did not affect the capacity of the scanning 43S PIC to discriminate against poor AUG context in TC mRNA in our system (Figure 3G, lanes 1, 2, 4, 6 and 8). Moreover, DHX29 reduced leaky scanning through the first AUG codon in the presence of any eIF1A variant in the same manner (Figure 3G, lanes 3, 5, 7 and 9). We also did not detect differences between eIF1A WT and mutants in AUG and near-cognate CUG recognition on the native β-globin mRNA (Figure 3H). The lack of an effect on start codon recognition for the eIF1A mutants could be explained by the different optimal AUG nucleotide context sequences between yeast and mammals, implying a less important role for the mammalian eIF1A NTT in AUG recognition. It would be difficult to evaluate the effect of DHX29 in our system in the presence of eIF1A CTT mutants because they already reduce the stringency of initiation codon selection. Therefore, we did not construct and test eIF1A CTT mutants. In conclusion, the eIF1A NTT does not contribute to start codon selection in our system, and DHX29 does not affect AUG recognition through the eIF1A NTT.

Contact between DHX29 and eIF1A is essential for DHX29-mediated codon selection

To test our hypothesis that DHX29 affects AUG selection through contact with eIF1A, we disrupted this contact and followed DHX29 activity. We found that the eIF1A-binding site is located within 1–247 aa of DHX29. For more precise contact localization, we employed the deletion approach and then tested mutants in our system. First, we constructed a set of N-terminal DHX29 deletion mutants: DHX29(Δ1–24), DHX29(Δ1–53), DHX29(Δ1–90), and DHX29(Δ1–124). Only DHX29(Δ1–24) and DHX29(Δ1–53) were soluble after expression in *E. coli* (Supplementary Figure S1A). These mutants influence AUG selection as efficiently as the WT protein (Supplementary Figure S1B). We also compared the eIF1A-binding capacity of WT and mutant DHX29. All forms of DHX29 bound to GST-eIF1A (OB) with equal efficiency (Supplementary Figure S1C). Due to the absence of structural data on the unique N-terminal part of DHX29, we divided the 247 aa into eight sections of 30 aa each and constructed internal deletion mutants with the removal of every odd numbered 30 aa section. Because we had already constructed DHX29(Δ1–24) and DHX29(Δ1–53) variants, we constructed DHX29(Δ61–90), DHX29(Δ121–150) and DHX29(Δ181–210) mutants. After expression, only the DHX29(Δ181–210) form was soluble (Figure 4A). In contrast to DHX29(WT), DHX29(Δ181–210) at different concentrations lost its dominant-negative effect on the poor-context discrimination of the scanning 43S PIC (Figure 4B).

To confirm the connection between the AUG selection defect and the eIF1A-binding capability of DHX29, we em-

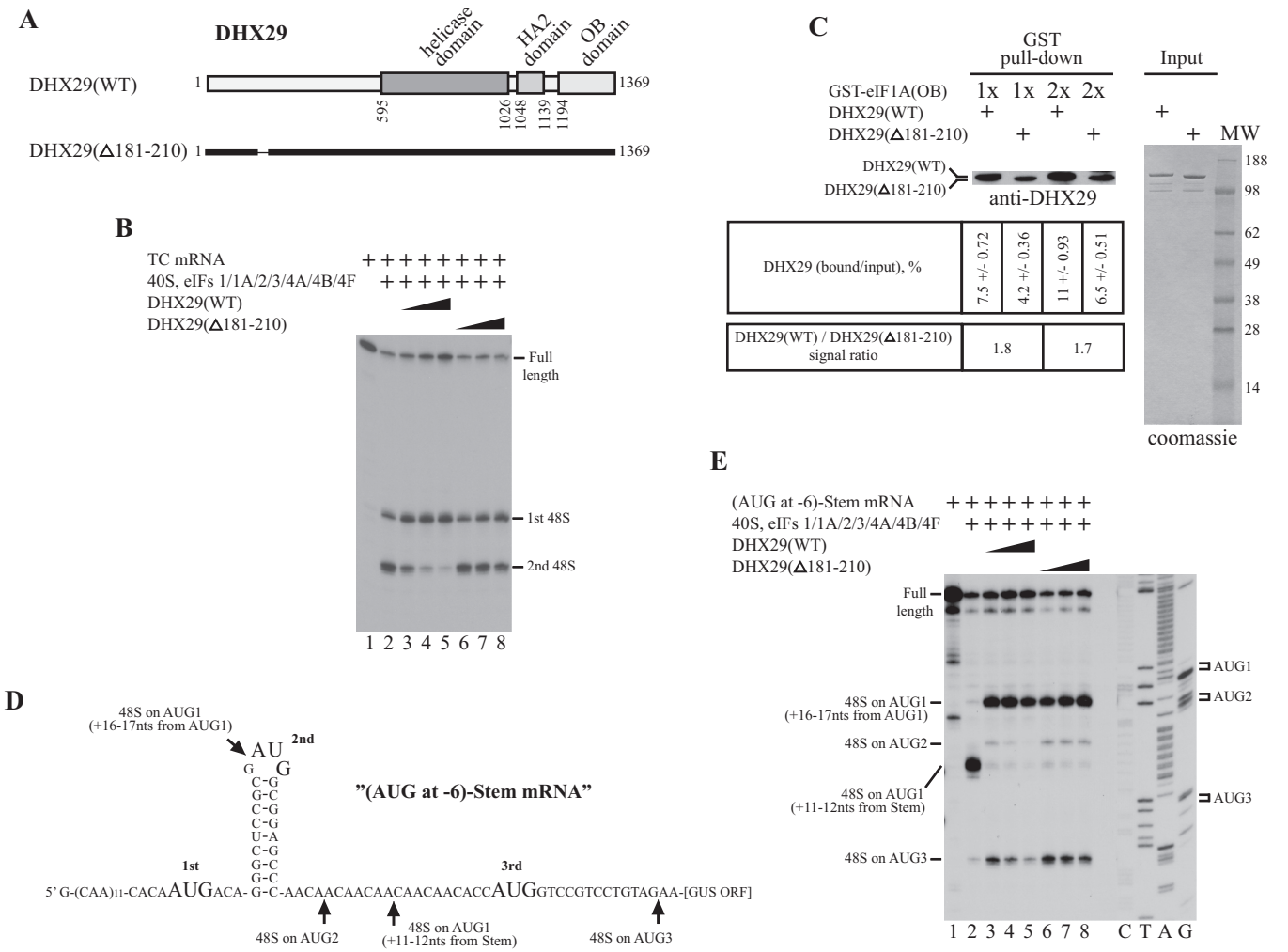

Figure 4. Role of contact between DHX29 and eIF1A in DHX29-mediated AUG recognition. (**A**) Organization of the DHX29(Δ181–210) deletion mutant. (**B**) Toeprint analysis of 48S IC assembly on TC mRNA in the presence of DHX29(Δ181–210). Positions of full-length signal and the assembled 48S IC are indicated. (**C**) Binding of DHX29(WT) and DHX29(Δ181–210) to eIF1A(OB) tested by GST pull-down assay. Appearance of input DHX29(WT) and DHX29(Δ181–210) was analyzed by SDS-PAGE and Coomassie blue staining. An aliquot of each binding reaction after elution from glutathione resin was assayed by SDS-PAGE and immunoblotting with anti-DHX29 antibodies. Positions of DHX29(WT), DHX29(Δ181–210) and molecular weight markers are shown. The ratios of eIF1A(OB)-bound DHX29 compared to DHX29 input ($n = 3$, mean ± SD) at two different concentrations of GST-eIF1A(OB) and the ratio of DHX29(WT)/(Δ181–210) signal intensities (mean/mean) are calculated. (**D**) Structure of (AUG at −6)-Stem mRNA. The positions of toeprint signals for the 48S ICs assembled on different start codons are indicated. (**E**) Toeprint analysis of 48S IC formation on (AUG at −6)-Stem mRNA in the presence of DHX29(WT) and DHX29(Δ181–210). Initiation codons and positions of the assembled 48S ICs are shown. Lanes C/T/A/G depict corresponding DNA sequences.

ployed GST pull-down assays (Figure 4C). We performed two serial dilutions of GST-eIF1A(OB) and calculated the mean value with standard deviation for DHX29 bound to GST-eIF1A(OB) as the percentage to DHX29 input for each dilution and each DHX29 form based on three replicate experiments. Then, for each GST-eIF1A(OB) dilution, we used an independent groups t-test for the comparison of DHX29(WT) and DHX29(Δ181–210) binding to GST-eIF1A(OB), and found that *P*-value is <0.05. This indicates a significant difference between DHX29(WT) and DHX29(Δ181–210) in binding to GST-eIF1A(OB). In conclusion, DHX29(Δ181–210) binds to GST-eIF1A(OB) less efficiently than DHX29(WT). The weak association of DHX29(Δ181–210) with GST-eIF1A(OB) could be explained by the incomplete removal of the eIF1A-binding site with the deletion approach. In conclusion, the contact between DHX29 and eIF1A is essential for DHX29-mediated codon selection.

DHX29 was originally discovered as a protein that stimulated 48S IC formation on mRNAs with highly structured 5′-UTRs. The direct test of the DHX29-mediated RNA unwinding activity of ribosomal complexes is 48S IC reconstitution on previously described (AUG at -6)-Stem mRNA (35). (AUG at -6)-Stem mRNA consists of a single-stranded region of (CAA) repeats with a centrally introduced 9 bp hairpin and three differently located AUG codons (Figure 4D). The first AUG (AUG1) is inserted upstream of a hairpin (A in AUG1 is at the '-6' position to a hairpin), the second AUG (AUG2) is in the loop of the hairpin, and the third AUG (AUG3) is located downstream of the hairpin. AUG3

is followed by the β-glucuronidase ORF. All AUGs are in an optimal nucleotide context.

In the presence of the canonical set of factors, the 48S IC was assembled on (AUG at -6)-Stem mRNA almost exclusively on AUG1 (Figure 4E, lanes 1 and 2). In the absence of DHX29, the stem remained intact, and the 43S PIC could not scan through it and reach AUG2 and AUG3, forming the 48S IC on AUG1 with the stem in the intact state, occupying the mRNA entry channel and producing the toeprint signal at the position +11–12 nt from the stem (Figure 4D and E, lane 2). The presence of DHX29 in different concentrations resulted in the complete unwinding of the hairpin, placing it in a single-stranded state in the mRNA binding channel of the 40S subunit and yielding the toeprint signal at a common position +16–17 nt from AUG1 (Figure 4D and E, lanes 3–5). Moreover, at the low concentration, DHX29 permitted the 43S PIC to scan through a hairpin in the unwound state and to form the 48S IC on AUG2 and AUG3 (Figure 4D and E, lane 3). These results are in good agreement with previously published data (35). Consistent with our experiments on TC mRNA, increases in the DHX29 concentration reduced 48S IC formation on AUG2 and AUG3 (Figure 4E, lanes 3–5). The presence of DHX29(Δ181-210) at different concentrations caused RNA secondary structure unwinding as efficiently as did DHX29(WT), as revealed by the shift from a '+11–12 nt from Stem' toeprint signal to a '+16–17 nt from AUG1' signal on (AUG at −6)-Stem mRNA (Figure 4E, lanes 6–8). Importantly, in the presence of either form of DHX29, the 43S PIC may scan through the DHX29-unwound stem and form the 48S IC on AUG2 and AUG3 (Figure 4E). However, in contrast to DHX29(WT), DHX29(Δ181-210) lost its dominant-negative effect on the poor-context discrimination role of the scanning 43S PIC. DHX29(Δ181–210) did not decrease leaky scanning through AUG1 of (AUG at −6)-Stem mRNA, and the amounts of 48S IC assembled on AUG2 and AUG3 upon addition of this mutant remained the same (Figure 4E, lanes 6–8). In conclusion, DHX29(Δ181-210) promoted mRNA secondary structure unwinding as efficiently as DHX29 (WT) but lost its activity in reducing leaky scanning through AUG compared to DHX29 (WT). Therefore, mutational analysis permitted us to separate the RNA-unwinding and AUG selection activities of DHX29.

DHX29 causes eIF1A and eIF2α rearrangement in key nucleotide context positions in ribosomal complexes

To obtain insights into the mechanism of DHX29 activity, we employed the directed UV crosslinking approach. The technique is based on the low-energy UV irradiation of mRNA with a co-transcriptionally introduced 4-thiouridine (4-thioU), resulting in the specific activation of 4-thioU for crosslinking. Because the start codon nucleotide context is an important determinant of the DHX29-mediated effect, in our experiments, we used two previously described (24,31) model '-3U' and '+4U' mRNAs consisting of (CAA) repeat-based 5′-UTRs, ORFs with one AUG codon, and a locally introduced single uridine in either the '−3' or '+4' key nucleotide context position, respectively (Figure 5A). These single-stranded mRNAs permit efficient 48S IC assembly in the reconstituted system (24,31). The 4-thioU at the +4 position of mRNA in the sucrose density gradient (SDG)-purified 48S IC crosslinks with ribosomal protein uS19 (according to novel universal nomenclature (40)), whereas 4-thioU at the −3 position crosslinks with eIF2α and ribosomal protein uS7 (31). Because eIF1A dissociates from ribosomal complexes during SDG centrifugation (41), to preserve the integrity of the process we irradiated the 48S IC immediately after assembly without purification by SDG centrifugation.

The 4-thioU at the +4 position of '+4U' mRNA in the 48S IC crosslinked more efficiently with eIF1A and less efficiently with uS19 (Figure 5B, lane 1). The presence of crosslinking to eIF1A is in agreement with the recently published CryoEM structure of the partial yeast 48S IC, where Trp70 of eIF1A interacts with the +4 mRNA base (9). In contrast to previous crosslinking data (31), we detected crosslinking to eIF1A because we omitted the SDG centrifugation step. eIF1A removal resulted in crosslinking exclusively to uS19 with substantially higher efficiency than with the full set of factors (Figure 5B, lane 4). The difference in crosslinking intensities to eIF1A may reflect two different conformational states of the mRNA entry channel. The addition of different DHX29 concentrations to the 48S IC did not affect crosslinking to uS19 but decreased crosslinking to eIF1A, most likely as a result of direct contact between these proteins, suggesting the rearrangement of eIF1A (Figure 5B, lanes 2 and 3).

In turn, 4-thioU at the −3 position of '−3U' mRNA crosslinked strongly to eIF2α and weakly to uS7 in the 48S IC (Figure 5C, lane 1), consistent with published data (31), and with approximately the same efficiency to both proteins in the absence of eIF1A (Figure 5C, lane 4). These data again reflect two different conformation states of the mRNA-binding channel of the 40S subunit. The addition of different DHX29 concentrations to the 48S IC did not change the uS7 signal but reduced eIF2α crosslinking (Figure 5C, lane 2 and 3). At the same time, DHX29 did not influence the affinity of eIF2 to the 43S PIC (11).

We quantified data shown in Figure 5B and C, and presented our calculations as eIF1A/uS19 (Figure 5B) and eIF2α/uS7 (Figure 5C) signal ratios. We indicated the mean value with standard deviation for each sample based on three replicate experiments. To confirm our conclusion that ribosomal binding of DHX29 affects mRNA crosslinking at the positions '+4' and '-3' to eIF1A and eIF2α, respectively, we employed an independent groups *t*-test. We compared eIF1A/uS19 or eIF2α/uS7 signal ratios obtained in the absence (lane 1) and in the presence of DHX29 at higher concentration (lane 3), and found that *P*-value in both *t*-tests is <0.05. This indicates a significant difference for eIF1A and eIF2α in mRNA crosslinking in the presence and in the absence of DHX29.

To assay whether the crosslinking pattern changes depend on contact between DHX29 and eIF1A, we compared the effects of DHX29(WT) and DHX29(Δ181–210) on the crosslinking of mRNA at the +4 and −3 positions to eIF1A and eIF2α, respectively. According to the signal intensity calculations, DHX29(Δ181-210) also reduced crosslinking to both proteins, but less than DHX29(WT) (Figure 5D and E).

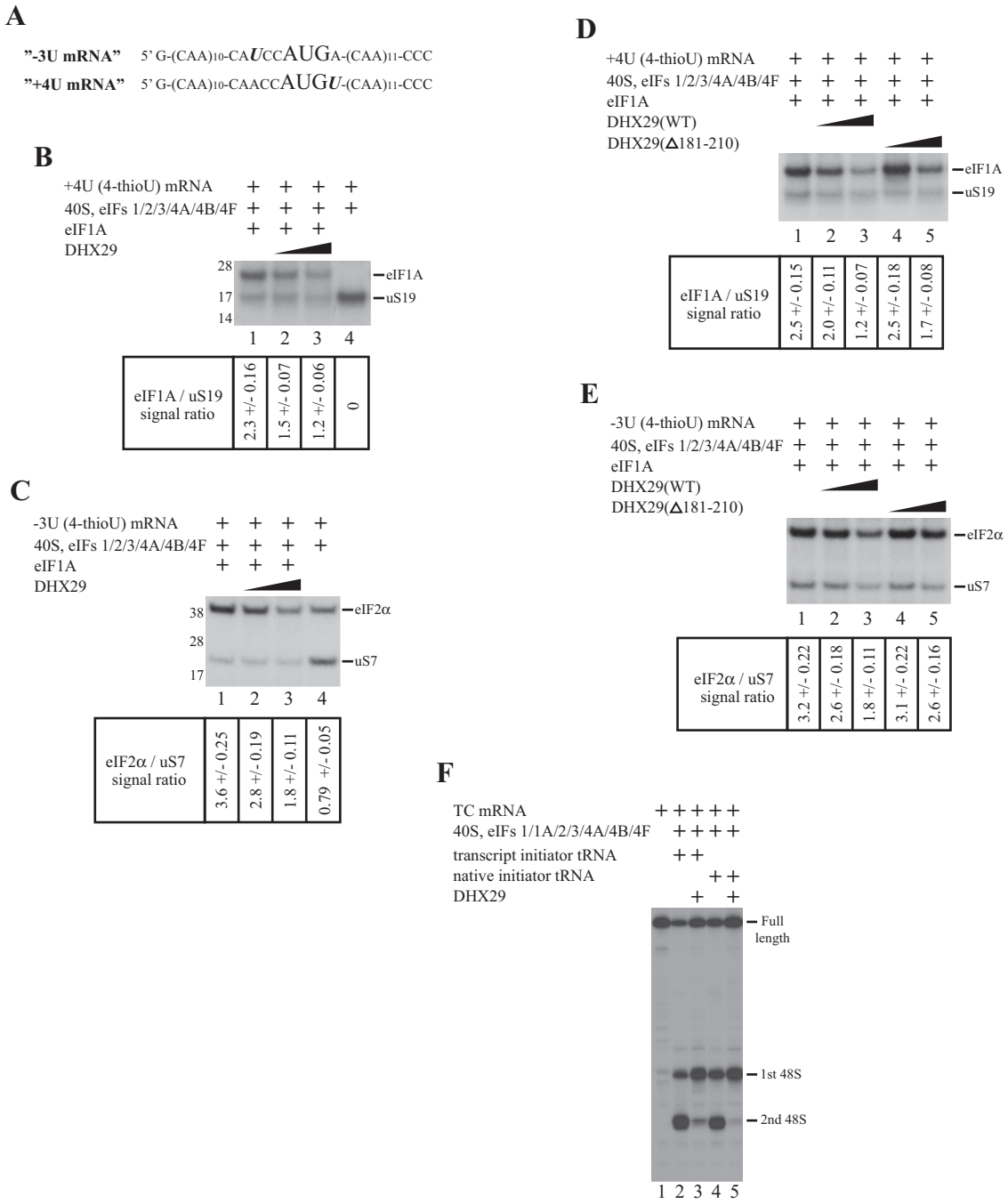

Figure 5. DHX29 affects crosslinking of eIF1A and eIF2α in initiation complexes. Role of initiator tRNA in the DHX29-mediated AUG selection. (**A**) Structures of '-3U' and '+4U' mRNAs. (**B** and **C**) UV crosslinking of 32P-labeled (B) '+4U' and (C) '−3U' mRNAs containing 4-thioU with components of assembled 48S ICs before and after incubation with DHX29, assayed by SDS-PAGE and autoradiography. Positions of crosslinked proteins and molecular weight markers are indicated. eIF1A/uS19 and eIF2α/uS7 ratios ($n = 3$, mean ± SD) are calculated. (**D** and **E**) Comparison of UV crosslinking of 32P-labeled (D) '+4U' and (E) '−3U' mRNAs containing 4-thioU with components of the reconstituted 48S IC after incubation with DHX29 (WT) or DHX29(Δ181-210), analyzed by SDS-PAGE and autoradiography. Positions of crosslinked proteins are shown. eIF1A/uS19 and eIF2α/uS7 ratios ($n = 3$, mean ± SD) are calculated. (**F**) Toeprint analysis of 48S IC formation on TC mRNA in the presence of different forms of initiator tRNA. Positions of full-length signal and assembled 48S ICs are indicated.

Our findings suggest that DHX29 may induce the rearrangement of eIF2α at the −3 mRNA position, consistent with the conformational variability of eIF2 in ribosomal complexes (12). According to CryoEM data (12), there is no direct contact between DHX29 and eIF2α in the 43S PIC. Therefore, DHX29 may transmit its effect through contacts with other 43S PIC components, including the detected DHX29-eIF1A contact. Taken together, it is tempting to speculate that upon binding to the 43S PIC, DHX29 causes eIF1A rearrangement through direct contact with the protein and indirectly rearranges eIF2α through the chain of contacts. In conclusion, we hypothesize that the observed rearrangements could underlie the mechanism of DHX29-mediated AUG selection.

Nucleotide modifications of initiator tRNA are not essential for the DHX29-mediated effect

Throughout the experiments, we used a transcript variant of initiator tRNA. Nucleotide modifications of tRNA fine-tune the molecular structure for optimal functional performance, thereby playing an important role in translation (42). We compared the transcript and native forms of initiator tRNA in our system. DHX29 affected AUG recognition on TC mRNA in the presence of native tRNA as efficiently as in the presence of transcript, suggesting that nucleotide modifications of initiator tRNA are not essential for DHX29-mediated AUG selection (Figure 5F).

DISCUSSION

Mammalian translation initiation is a complex process with multiple components. Efficient and accurate 48S IC formation on the mRNA initiation codon is achieved through numerous contacts between translational apparatus components. The DExH-box helicase DHX29 is a recently discovered initiation factor that was fractionated as a protein that stimulated ribosomal scanning on mRNAs with structured 5′-UTRs. Although many initiation factors exhibit various activities during translation initiation, only one activity has been assigned to DHX29. Recent CryoEM data of the ribosomal position of DHX29 in the mammalian 43S PIC shed light on its binding partners. The major density around helix H16, representing the helicase and C-terminal parts of DHX29, establishes contacts with eIF3b and eIF3i subunits of eIF3, whereas the minor distal density is located next to the eIF1A-binding site. In the present work, we studied the potential interplay between mammalian-specific DHX29 and eIF1A and its role in AUG selection. To this end, we employed a reconstituted in vitro mammalian translational system in combination with mutational analysis and biochemical techniques and found that DHX29 reduces leaky scanning through uAUG but not near-cognate uCUG regardless of nucleotide context. The contact between DHX29 and eIF1A is essential for the DHX29-mediated effect.

Employing GST pull-down assays, we demonstrated and localized the contact between the first half of the N-terminal region of DHX29 and the OB domain of eIF1A. This finding unambiguously assigned the distal density of DHX29 to the N-terminal part of the protein, which had not yet been assigned due to the absence of the DHX29 crystal structure. Comparative analysis has not revealed any conserved motifs/domains in the N-terminal part of protein, which is approximately 600 aa long, making it unique for the protein. Moreover, computer modeling does not detect extensive structural elements/ensembles in this region. Therefore, it is tempting to speculate that this structural organization explains the flexibility of the N-terminal part of DHX29 in the 43S PIC and that the stabilization of the distal part of the N-terminus only occurs as a result of contact with eIF1A.

Because DHX29 is located aside from the active center of the 40S subunit, it could indirectly affect AUG selection. On the other hand, several components of our system are directly involved in AUG selection. We found that DHX29 did not cause the dissociation of eIFs 1 or 1A, as revealed in toeprint assays on different mRNAs. Notably, we detected that in the absence of eIF1A, DHX29 blocked 43S PIC loading onto mRNA. This finding is in good agreement with CryoEM data, where DHX29 establishes a bridge between the body and the beak of the 40S subunit near the mRNA entry channel latch. Importantly, this structure does not contain eIFs 1 and 1A and may reflect, at least in part, our situation when eIF1A was omitted in the system. Therefore, this physical barrier could block mRNA access to the mRNA entry channel, which could explain our finding. This interesting DHX29 activity may prevent the incomplete 43S PIC from participating in downstream events during translation initiation, thereby preserving the energy of the system.

DHX29 establishes contact with eIF1A, a key player in the fidelity of AUG selection. Therefore, our next hypothesis was that DHX29 acts through eIF1A. In our system, eIF1A NTT mutants are as efficient in 48S IC formation and DHX29 activity as eIF1A(WT), suggesting that DHX29 activity is not transmitted through the eIF1A NTT. Another interesting finding is that the eIF1A NTT is less important for 48S IC stabilization in our mammalian system than in yeast cells. Unfortunately, we could not test the eIF1A CTT in the DHX29 effect because eIF1A CTT mutants already exhibited reduced stringency in AUG selection.

Employing mutational analysis, we identified the 30-aa deletion mutant DHX29(Δ181-210) with impaired AUG selection function, although its RNA unwinding activity remained completely intact. Compared to DHX29(WT), DHX29(Δ181-210) showed less affinity for eIF1A, implying that DHX29-eIF1A contact is essential for DHX29 activity. These findings confirm that AUG selection and RNA unwinding are two different and unrelated functions of DHX29, and we have discovered the novel role of this protein in translation initiation.

To obtain insights into the mechanism of DHX29-mediated AUG selection, we followed crosslinking patterns in the '−3' and '+4' key nucleotide context positions of mRNA in reconstituted initiation complexes. We found that the '+4' nucleotide crosslinked strongly to eIF1A and slightly to uS19 in the complete 48S IC and highly efficiently to uS19 in the 48S IC reconstituted in the absence of eIF1A. The crosslinking patterns reflect the two different conformational states of the mRNA entry channel of the 40S sub-

unit in the presence and absence of eIF1A. The contact between the '+4' base and eIF1A correlates with yeast data, implying similar local architecture of the 48S IC between yeast and mammals. DHX29 does not change the intensity of the uS19 crosslinking signal, suggesting that it does not induce the conformational changes in the 40S subunit upon binding. However, DHX29 decreases crosslinking to eIF1A, most likely as a result of direct contact between these proteins, assuming the rearrangement of eIF1A. In turn, the '−3' base crosslinks more strongly to eIF2α and weakly to uS7 in the complete 48S IC and with equal efficiency to both proteins in the absence of eIF1A. These data confirm our conclusion regarding the two different conformational states of the mRNA entry channel in the presence and absence of eIF1A. The addition of DHX29 decreases eIF2α crosslinking. eIF2α rearrangement is not surprising because this protein reveals the conformational variability in initiation complexes depending on the complex composition. In other words, this variability depends on the mutual orientation of the head and the body of the 40S subunit, which is different between the open scanning-competent and closed scanning-arrested conformational states of the 40S subunit.

In summary, we propose two equally likely alternative hypotheses for the mechanism underlying the DHX29-mediated effect. During mammalian translation initiation, DHX29 binds to the 43S PIC and establishes the contact between the first half of its N-terminal part and the OB domain of eIF1A. At this moment, we cannot unambiguously conclude when DHX29 contacts eIF1A. Because DHX29 binds to the 40S subunit, the 43S PIC and the 48S IC with high affinity (11), we suggest that DHX29 may establish contact with eIF1A at any step during initiation. According to the first hypothesis, upon ribosomal binding, DHX29 causes the rearrangement of eIF1A and eIF2α in key nucleotide context positions of the initiation complex. We suggest that the eIF1A CTT slightly changes its position in the P site due to this rearrangement and begins to play a less important role in the stabilization of the open scanning-competent conformation of the 43S PIC. As a result, the 43S PIC reduces leaky scanning through uAUG. According to the second hypothesis, upon ribosomal binding, DHX29 changes the architecture of the mRNA-binding channel. This rearrangement results in the stabilization of the closed conformation of the 43S PIC only with the perfect codon-anticodon duplex formed at AUG in the P site, regardless of the context nucleotides, leading to decreased leaky scanning through uAUG. Indeed, DHX29 not only promotes the recognition of uAUG independent of its context but also fails to stimulate the recognition of near cognates. This behavior distinguishes its effect on the start codon recognition from the opposing function of eIF1, which discriminates against both near-cognates and AUGs in the poor context. The contact between DHX29 and eIF1A is important for the stabilization of the flexible N-terminal part of DHX29 near the mRNA entrance. The altered conformations of eIF1A and eIF2a evoked by DHX29 are only relevant to the DHX29-mediated event and are not involved in discriminating against AUGs in poor Kozak context or near-cognate start sites. What are the implications of these findings? Many native mRNAs contain one or more uAUGs, which often play regulatory roles in translation initiation, and annotated initiation codons are not always in the optimal context. Therefore, the described activity of DHX29 should affect the expression levels of such mRNAs.

SUPPLEMENTARY DATA

Supplementary Data are available at NAR Online.

ACKNOWLEDGEMENTS

We thank Tatyana Pestova for the (AUG at −6) mRNA transcription vector and Anton Komar for the DHX29 expression vector.

FUNDING

National Institutes of General Medical Sciences [GM097014 to A.V.P.]. Funding for open access charge: National Institutes of Health [GM097014 to A.V.P.].
Conflict of interest statement. None declared.

REFERENCES

1. Hinnebusch,A.G. (2011) Molecular mechanism of scanning and start codon selection in eukaryotes. *Microbiol. Mol. Biol. Rev.*, **75**, 434–467.
2. Jackson,R.J., Hellen,C.U.T. and Pestova,T.V. (2010) The mechanism of eukaryotic translation initiation and principles of its regulation. *Nat. Rev. Mol. Cell Biol.*, **11**, 113–127.
3. Maag,D. and Lorsch,J.R. (2003) Communication between eukaryotic translation initiation factors 1 and 1A on the yeast small ribosomal subunit. *J. Mol. Biol.*, **330**, 917–924.
4. Lomakin,I.B. and Steitz,T.A. (2013) The initiation of mammalian protein synthesis and mRNA scanning mechanism. *Nature*, **500**, 307–311.
5. Weisser,M., Voigts-Hoffmann,F., Rabl,J., Leibundgut,M. and Ban,N. (2013) The crystal structure of the eukaryotic 40S ribosomal subunit in complex with eIF1 and eIF1A. *Nat. Struct. Mol. Biol.*, **20**, 1015–1017.
6. Passmore,L.A., Schmeing,T.M., Maag,D., Applefield,D.J., Acker,M.G., Algire,M.A., Lorsch,J.R. and Ramakrishnan,V. (2007) The eukaryotic translation initiation factors eIF1 and eIF1A induce an open conformation of the 40S ribosome. *Mol. Cell*, **26**, 41–50.
7. Rabl,J., Leibundgut,M., Ataide,S.F., Haag,A. and Ban,N. (2011) Crystal structure of the eukaryotic 40S ribosomal subunit in complex with initiation factor 1. *Science*, **331**, 730–736.
8. Saini,A.K., Nanda,J.S., Lorsch,J.R. and Hinnebusch,A.G. (2010) Regulatory elements in eIF1A control the fidelity of start codon selection by modulating tRNA(i)(Met) binding to the ribosome. *Genes Dev.*, **24**, 97–110.
9. Hussain,T., Llácer,J.L., Fernández,I.S., Munoz,A., Martin-Marcos,P., Savva,C.G., Lorsch,J.R., Hinnebusch,A.G. and Ramakrishnan,V. (2014) Structural changes enable start codon recognition by the eukaryotic translation initiation complex. *Cell*, **159**, 597–607.
10. Parsyan,A., Shahbazian,D., Martineau,Y., Petroulakis,E., Alain,T., Larsson,O., Mathonnet,G., Tettweiler,G., Hellen,C.U., Pestova,T.V. *et al.* (2009) The helicase protein DHX29 promotes translation initiation, cell proliferation, and tumorigenesis. *Proc. Natl. Acad. Sci. U.S.A.*, **106**, 22217–22222.
11. Pisareva,V.P., Pisarev,A.V., Komar,A.A., Hellen,C.U.T. and Pestova,T.V. (2008) Translation initiation on mammalian mRNAs with structured 5′ UTRs requires DExH-box protein DHX29. *Cell*, **135**, 1237–1250.
12. Hashem,Y., des Georges,A., Dhote,V., Langlois,R., Liao,H.Y., Grassucci,R.A., Hellen,C.U.T., Pestova,T.V. and Frank,J. (2013) Structure of the mammalian ribosomal 43S preinitiation complex bound to the scanning factor DHX29. *Cell*, **153**, 1108–1119.

13. Kozak,M. (1987) An analysis of 5′-noncoding sequences from 699 vertebrate messenger RNAs. *Nucleic Acids Res.*, **15**, 8125–8148.
14. Maag,D., Fekete,C.A., Gryczynski,Z. and Lorsch,J.R. (2005) A conformational change in the eukaryotic translation preinitiation complex and release of eIF1 signal recognition of the start codon. *Mol. Cell*, **17**, 265–275.
15. Cheung,Y.-N., Maag,D., Mitchell,S.F., Fekete,C.A., Algire,M.A., Takacs,J.E., Shirokikh,N., Pestova,T., Lorsch,J.R. and Hinnebusch,A.G. (2007) Dissociation of eIF1 from the 40S ribosomal subunit is a key step in start codon selection in vivo. *Genes Dev.*, **21**, 1217–1230.
16. Algire,M.A., Maag,D. and Lorsch,J.R. (2005) Pi release from eIF2, not GTP hydrolysis, is the step controlled by start-site selection during eukaryotic translation initiation. *Mol. Cell*, **20**, 251–262.
17. Nanda,J.S., Cheung,Y.-N., Takacs,J.E., Martin-Marcos,P., Saini,A.K., Hinnebusch,A.G. and Lorsch,J.R. (2009) eIF1 controls multiple steps in start codon recognition during eukaryotic translation initiation. *J. Mol. Biol.*, **394**, 268–285.
18. Noderer,W.L., Flockhart,R.J., Bhaduri,A., Diaz de Arce,A.J., Zhang,J., Khavari,P.A. and Wang,C.L. (2014) Quantitative analysis of mammalian translation initiation sites by FACS-seq. *Mol. Syst. Biol.*, **10**, 748.
19. Mouilleron,H., Delcourt,V. and Roucou,X. (2016) Death of a dogma: eukaryotic mRNAs can code for more than one protein. *Nucleic Acids Res.*, **44**, 14–23.
20. Kozak,M. (2002) Emerging links between initiation of translation and human diseases. *Mamm. Genome*, **13**, 401–410.
21. Wolf,A., Caliebe,A., Thomas,N.S.T., Ball,E.V., Mort,M., Stenson,P.D., Krawczak,M. and Cooper,D.N. (2011) Single base-pair substitutions at the translation initiation sites of human genes as a cause of inherited disease. *Hum. Mutat.*, **32**, 1137–1143.
22. Xu,H., Wang,P., You,J., Zheng,Y., Fu,Y., Tang,Q., Zhou,L., Wei,Z., Lin,B., Shu,Y. *et al.* (2010) Screening of Kozak-motif-located SNPs and analysis of their association with human diseases. *Biochem. Biophys. Res. Commun.*, **392**, 89–94.
23. Elantak,L., Wagner,S., Herrmannová,A., Karásková,M., Rutkai,E., Lukavsky,P.J. and Valásek,L. (2010) The indispensable N-terminal half of eIF3j/HCR1 cooperates with its structurally conserved binding partner eIF3b/PRT1-RRM and with eIF1A in stringent AUG selection. *J. Mol. Biol.*, **396**, 1097–1116.
24. Pisareva,V.P. and Pisarev,A.V. (2014) eIF5 and eIF5B together stimulate 48S initiation complex formation during ribosomal scanning. *Nucleic Acids Res.*, **42**, 12052–12069.
25. Saini,A.K., Nanda,J.S., Martin-Marcos,P., Dong,J., Zhang,F., Bhardwaj,M., Lorsch,J.R. and Hinnebusch,A.G. (2014) Eukaryotic translation initiation factor eIF5 promotes the accuracy of start codon recognition by regulating Pi release and conformational transitions of the preinitiation complex. *Nucleic Acids Res.*, **42**, 9623–9640.
26. Terenin,I.M., Akulich,K.A., Andreev,D.E., Polyanskaya,S.A., Shatsky,I.N. and Dmitriev,S.E. (2015) Sliding of a 43S ribosomal complex from the recognized AUG codon triggered by a delay in eIF2-bound GTP hydrolysis. *Nucleic Acids Res.*, **44**, 1882-1893.
27. Kochetov,A.V. (2008) Alternative translation start sites and hidden coding potential of eukaryotic mRNAs. *Bioessays*, **30**, 683–691.
28. Kozak,M. (1999) Initiation of translation in prokaryotes and eukaryotes. *Gene*, **234**, 187–208.
29. Kozak,M. (2002) Pushing the limits of the scanning mechanism for initiation of translation. *Gene*, **299**, 1–34.
30. Wang,X.-Q. and Rothnagel,J.A. (2004) 5′-untranslated regions with multiple upstream AUG codons can support low-level translation via leaky scanning and reinitiation. *Nucleic Acids Res.*, **32**, 1382–1391.
31. Pisarev,A.V., Kolupaeva,V.G., Pisareva,V.P., Merrick,W.C., Hellen,C.U.T. and Pestova,T.V. (2006) Specific functional interactions of nucleotides at key -3 and +4 positions flanking the initiation codon with components of the mammalian 48S translation initiation complex. *Genes Dev.*, **20**, 624–636.
32. Aylett,C.H.S., Boehringer,D., Erzberger,J.P., Schaefer,T. and Ban,N. (2015) Structure of a yeast 40S-eIF1-eIF1A-eIF3-eIF3j initiation complex. *Nat. Struct. Mol. Biol.*, **22**, 269–271.
33. Pisarev,A.V., Hellen,C.U.T. and Pestova,T.V. (2007) Recycling of eukaryotic posttermination ribosomal complexes. *Cell*, **131**, 286–299.
34. Pisareva,V.P., Skabkin,M.A., Hellen,C.U.T., Pestova,T.V. and Pisarev,A.V. (2011) Dissociation by Pelota, Hbs1 and ABCE1 of mammalian vacant 80S ribosomes and stalled elongation complexes. *EMBO J.*, **30**, 1804–1817.
35. Abaeva,I.S., Marintchev,A., Pisareva,V.P., Hellen,C.U.T. and Pestova,T.V. (2011) Bypassing of stems versus linear base-by-base inspection of mammalian mRNAs during ribosomal scanning. *EMBO J.*, **30**, 115–129.
36. Pestova,T.V., Borukhov,S.I. and Hellen,C.U. (1998) Eukaryotic ribosomes require initiation factors 1 and 1A to locate initiation codons. *Nature*, **394**, 854–859.
37. Pestova,T.V. and Kolupaeva,V.G. (2002) The roles of individual eukaryotic translation initiation factors in ribosomal scanning and initiation codon selection. *Genes Dev.*, **16**, 2906–2922.
38. Fekete,C.A., Mitchell,S.F., Cherkasova,V.A., Applefield,D., Algire,M.A., Maag,D., Saini,A.K., Lorsch,J.R. and Hinnebusch,A.G. (2007) N- and C-terminal residues of eIF1A have opposing effects on the fidelity of start codon selection. *EMBO J.*, **26**, 1602–1614.
39. Luna,R.E., Arthanari,H., Hiraishi,H., Akabayov,B., Tang,L., Cox,C., Markus,M.A., Luna,L.E., Ikeda,Y., Watanabe,R. *et al.* (2013) The interaction between eukaryotic initiation factor 1A and eIF5 retains eIF1 within scanning preinitiation complexes. *Biochemistry*, **52**, 9510–9518.
40. Ban,N., Beckmann,R., Cate,J.H.D., Dinman,J.D., Dragon,F., Ellis,S.R., Lafontaine,D.L.J., Lindahl,L., Liljas,A., Lipton,J.M. *et al.* (2014) A new system for naming ribosomal proteins. *Curr. Opin. Struct. Biol.*, **24**, 165–169.
41. Unbehaun,A., Borukhov,S.I., Hellen,C.U.T. and Pestova,T.V. (2004) Release of initiation factors from 48S complexes during ribosomal subunit joining and the link between establishment of codon-anticodon base-pairing and hydrolysis of eIF2-bound GTP. *Genes Dev.*, **18**, 3078–3093.
42. Yarian,C., Townsend,H., Czestkowski,W., Sochacka,E., Malkiewicz,A.J., Guenther,R., Miskiewicz,A. and Agris,P.F. (2002) Accurate translation of the genetic code depends on tRNA modified nucleosides. *J. Biol. Chem.*, **277**, 16391–16395.